Radar time series analysis over West Anatolia

Arikan, Mahmut; Hooper, Andy; Hanssen, Ramon

Publication date
2010

Published in
Fringe 2009 Proceedings

Citation (APA)
Arikan, M., Hooper, A., & Hanssen, R. (2010). Radar time series analysis over West Anatolia. In H. Lacoste-Francis (Ed.), *Fringe 2009 Proceedings* (Vol. SP 677, pp. 1-6). (ESA SP; Vol. 677). ESA.

RADAR TIME SERIES ANALYSIS OVER WEST ANATOLIA

Mahmut Arıkan, Andrew Hooper, and Ramon Hanssen

Delft Institute of Earth Observation and Space Systems (DEOS), Delft University of Technology, Kluyverweg 1, 2629 HS, Delft, The Netherlands. Email:(M.Arikan, A.J.Hooper, R.F.Hanssen)@tudelft.nl

ABSTRACT

Interseismic tectonic motion manifests itself as a long (10's to 100's km) wavelength signal. The magnitude and the extent of the signal is crucial to understand kinematics of the crustal motion. For two decades, GPS measurements have been the main source of information for observing such a signal. In this study we use Persistent Scatterer Interferometry (PSI) observations, which provides better spatial resolution, to monitor tectonic signal over West Anatolia. The region is characterized by horst-graben morphology which is controlled by oblique-slip normal faults. The faults cause an extension circa 25-30 mm/yr in NE-SW direction as observed by sparse GPS network measurements. In our analysis, we have used 42 ERS images acquired between 1992 and 2001 years. We have identified coherent interferograms which would reduce the noise level in the rural areas leading to increased point density. Finally we compare our PSI results with two other GPS studies within the region. The modeled interseismic signal from a recent GPS study ([1]) agrees with the one modeled from that of PSI observations in trend direction.

Key words: InSAR, Persistent Scatterer Interferometry, interseismic deformation, West Anatolia.

1. INTRODUCTION

The Anatolian continental crust is continuously undergoing strain due to the collision of three major tectonic plates: the Eurasian, African and Arabian plates. This produced a complex tectonic setting: compressional tectonics in the East, strike-slip tectonics in the North and extensional tectonics in the West. The interaction of these major plates has caused the Anatolian block to rotate counter-clockwise towards the Hellenic trench since the late Miocene [5].

Here, we focus on the part of the West Anatolia region where geological structures are dominated by a horst-graben morphology, controlled by oblique-slip normal faults, see Figure 1(a). Recent GPS studies show that the region is extending circa 25-30 mm/yr in the NE-SW direction [11, 12]. In this study, using InSAR observation we attempt to quantify the magnitude and extend of the deforming crust along the West Anatolian Graben system and identify possible active faulting.

In the last decade radar time series techniques, such as DePSI, StaMPS, and StuN produce invaluable results to monitor ground deformation [10, 7, 9, 6]. However in rural areas where there is a low signal to noise ratio (SNR$<$10) PS density decreases and this makes it difficult to estimate the parameters of interest.

In this study, we present our approach to improve PS point density in the rural areas of West Anatolia for monitoring interseismic displacement. For our analysis we used 42 ERS 1/2 images of track 362 and frame 2835 acquired between 1992 to 2001, which covers part of Gediz (Alaşehir) Graben, Küçük Menderes Graben and Büyük Menderes Graben. The region is rather sparsely populated with towns and small villages along the basins, and the land is mainly used for agriculture and forestry. The topography is quite rough from 70 meters up to 2000 meters high, see Figure 1(b).

2. METHOD AND ANALYSIS

2.1. Forward Projection of GPS velocities in the Radar Line-of-Sight

We use GPS observations to obtain a first indication of interseismic displacement. Usually this is necessary to derive assumptions and refine our model equations. Using the displacement measurements of two recent GPS studies [12] (spanning 1988–2001 periods) and [1] (spanning 1997–2006 periods), we mapped the horizontal displacement vectors to the radar line-of-sight (LOS) of a descending acquisition geometry. In this study, we will refer to [12] and [1] as the GPS-1 and GPS-2 studies, respectively. Let the surface displacement orthogonal components be $D = (d_x, d_y, d_z)^T$, in east, north, and vertical (up) directions, respectively, for a given point at the Earth's surface. Then, the projection of the surface displacement vector D to the line of sight can be formulated as:

Proc. 'Fringe 2009 Workshop', Frascati, Italy, 30 November – 4 December 2009 (ESA SP-677, March 2010)

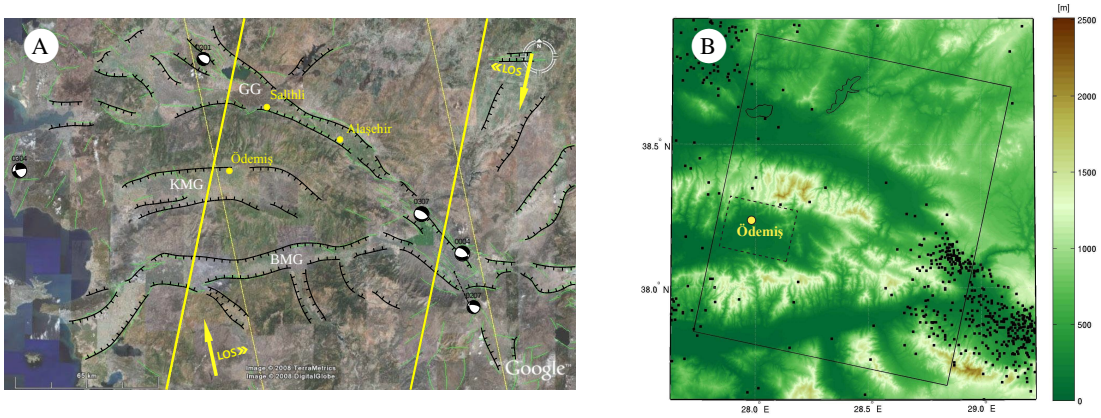

Figure 1. (a) Ascending and descending satellite passes over major horst-graben structures in West Anatolia: Gediz Graben (GG), Küçük Menderes Graben (KMG) and Büyük Menderes Graben (BMG). The structures are controlled mainly by oblique-slip normal faults. (b) Topography and seismicity surrounding the grabens. Square dots depict epicenters of the earthquakes having magnitude $M_w > 3$ within the region for the period 1990-2009 (B.U. KOERI, 2009). The dash box outlines the test site covering Ödemiş town.

$$d_{\text{LOS}} = s^T \cdot D \tag{1}$$

$$s = (-\cos\alpha_h \sin\theta \quad \sin\alpha_h \sin\theta \quad cos\theta)^T \tag{2}$$

Where d_{LOS}, s and D denote the line-of-sight displacement, the satellite unit vector, and the surface displacement vector, respectively. For detailed description of the satellite unit vector and its parameters see [2].

We use master acquisition parameters for heading, α_h, and incidence angle, θ, of an ERS descending pass. The result of the forward projection is illustrated in Figure 4(a) and 4(d). Both line-of-sight projections indicate a trend in N-S direction. This is due to lack of vertical displacement component in the GPS measurements and low sensitivity to the North component of displacement of the radar satellite orbit.

In order to simplify comparison of GPS and PSI measurements, using a bi-linear model we estimated interseismic signal from the LOS projections of GPS-1 and GPS-2 studies as indicated in Figure 4(a) and 4(d), respectively. Model estimates and residuals are illustrated in Figure 4(b) and 4(c), Figure 4(e) and 4(f) for GPS-1 and GPS-2 studies, respectively.

2.2. Radar Time Series Analysis

Our radar times series analysis uses coherent and usually strong scatterers, known as Persistent Scatterers (PS), that provide coherent phase information over time for monitoring scatterer movement. In areas with high (>10) signal to noise (SNR) ratio, such as urban areas, there is a sufficiently high density of coherent targets. On the other hand, in non-urban areas, due to change of backscattering

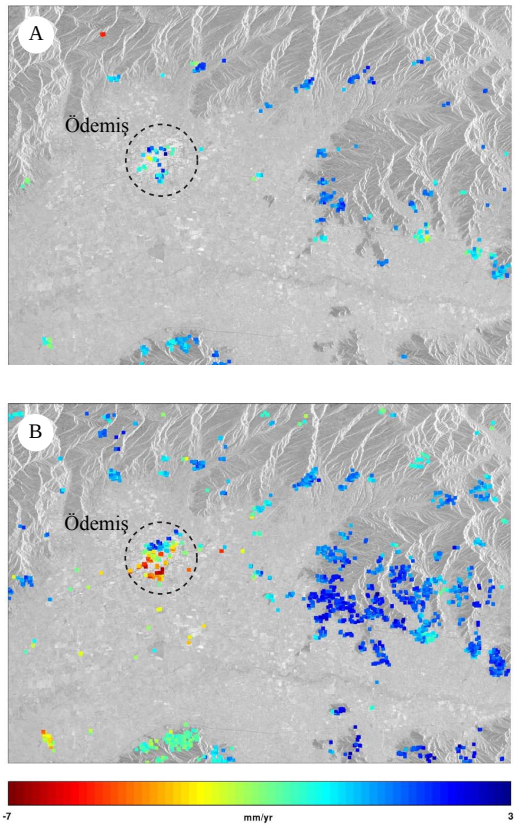

Figure 2. (a) 417 PS points detected using full resolution SAR image, overlaying mean amplitude image. (b) 2029 PS points detected using oversampled SAR images with a factor of two, overlaying mean amplitude image. The cluster of points indicates the location of Ödemiş town.

characteristics of scatterers, time series techniques may fail to pick enough coherent targets in order to produce reliable results. This is because a low density of coherent targets makes it difficult to estimate parameters of interest, such as atmospheric phase contribution, deformation, and dem error, in a stack of interferograms.

In our PSI processing, a full scene covering West Anatolia grabens is analyzed using a series of 42 ERS images spanning the period November 1992 to December 2000. The master acquisition is chosen to be orbit 18226 (Oct 1998), providing maximum expected coherence for the whole series of interferograms. This is computed based on the perpendicular baselines, the temporal baselines and the mean Doppler centroid frequency differences.

First, using 41 computed interferograms, we select an initial set of PS points based on a rather high amplitude dispersion compared to studies done in urban areas [6]. Among these points we identify coherent targets by first using a spatial window, we estimate noise for each candidate, using the noise term we compute coherence over time. Those points which have high coherence are kept, since they are likely to have stable phase behavior over time [8]. After this analysis we proceed to the estimation of the parameters.

Additionally, we considered the influence of the sub-pixel positions of scatterers where phase centers may not align exactly with the pixel center. For this reason we oversampled each SLC image with a factor two. In this way, we expect to improve the signal to noise ratio by better estimation of scatterer phase center, especially in the rural areas which suffer from low PS density, see Figure 2.

More over, using the best 100 PS points, which were identified based on very low amplitude dispersion threshold, we compute spatial coherence with a window size of 40 by 10 for every interferometric combination.

Then using the computed coherence matrices for each PS point, we estimate an expected coherence matrix for each baseline, i.e. Doppler, perpendicular, and temporal baselines [3]. This coherence matrix is then used to identify interferogram combinations that suffer from considerable decorrelation that could be related to a high Doppler centroid, large perpendicular baseline, and/or large time separation, or some other reason. This allows us to identify and eliminate noisy interferograms from our analysis. Figure 3 illustrates the coherence matrix of interferograms sorted based on perpendicular baseline.

This approach ensures that we use the maximum amount of available coherent acquisitions for parameter estimation, which makes it most reliable. After oversampling and eliminating noisy interferograms, PS density considerably increases in the full scene covering rural areas.

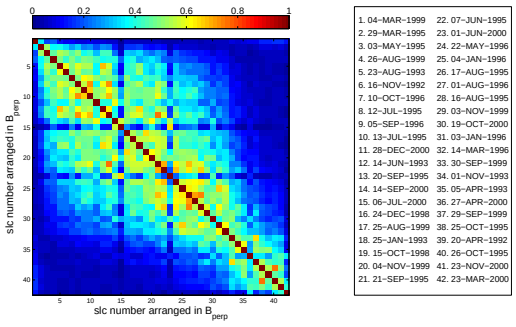

Figure 3. Expected coherence sorted on perpendicular baseline B_{perp}, estimated using best 100 PS points with a 40x10 spatial window size.

Table 1. List of ERS datasets found to be have low coherence over time.

Date	$B_{\perp}$(m)	B_{temp}(day)	B_{dopp}(hz)	Sat.
20-Apr-1992	963	-2369	261	ERS-1
05-Apr-1993	728	-2019	273	ERS-1
01-Nov-1993	6408	-1809	253	ERS-1
25-Oct-1995	903	-1086	179	ERS-2
26-Oct-1995	992	-1085	-41	ERS-2
04-Mar-1999	-1128	140	50	ERS-2
29-Sep-1999	805	349	277	ERS-1
30-Sep-1999	583	350	25	ERS-2
23-Mar-2000	1213	525	-387	ERS-2
27-Apr-2000	774	560	-264	ERS-2
01-Jun-2000	104	595	-440	ERS-2
06-Jul-2000	-92	630	-539	ERS-2
23-Nov-2000	120	770	-32	ERS-2

3. RESULTS AND DISCUSSION

Using a forward projection on the GPS data, we translated horizontal ground motions to the satellite LOS assuming no elevation change, since GPS data was lacking elevation measurements. This lead us to simplify our equations by dropping the terms relating to the vertical displacement vector.

In our PSI processing, first, we analyzed oversampled dataset using a small crop covering Ödemiş town, which is situated the inside Küçük Menderes graben. The region is rural and mostly populated with distributed scatterers. In our PSI analysis, initially we detected 417 coherent targets using full resolution SAR images, and later using the oversampled dataset, the number of PS is increased to 2029 points.

Following that, using the expected coherence matrix, see Figure 3 for an example of a coherence matrix sorted on of perpendicular baseline, we have identified 13 acquisitions that show higher decorrelation than the rest of images in the stack. These acquisitions were eliminated in PSI processing and are listed in table 1. In a full scene processing, initially, we detected 64385

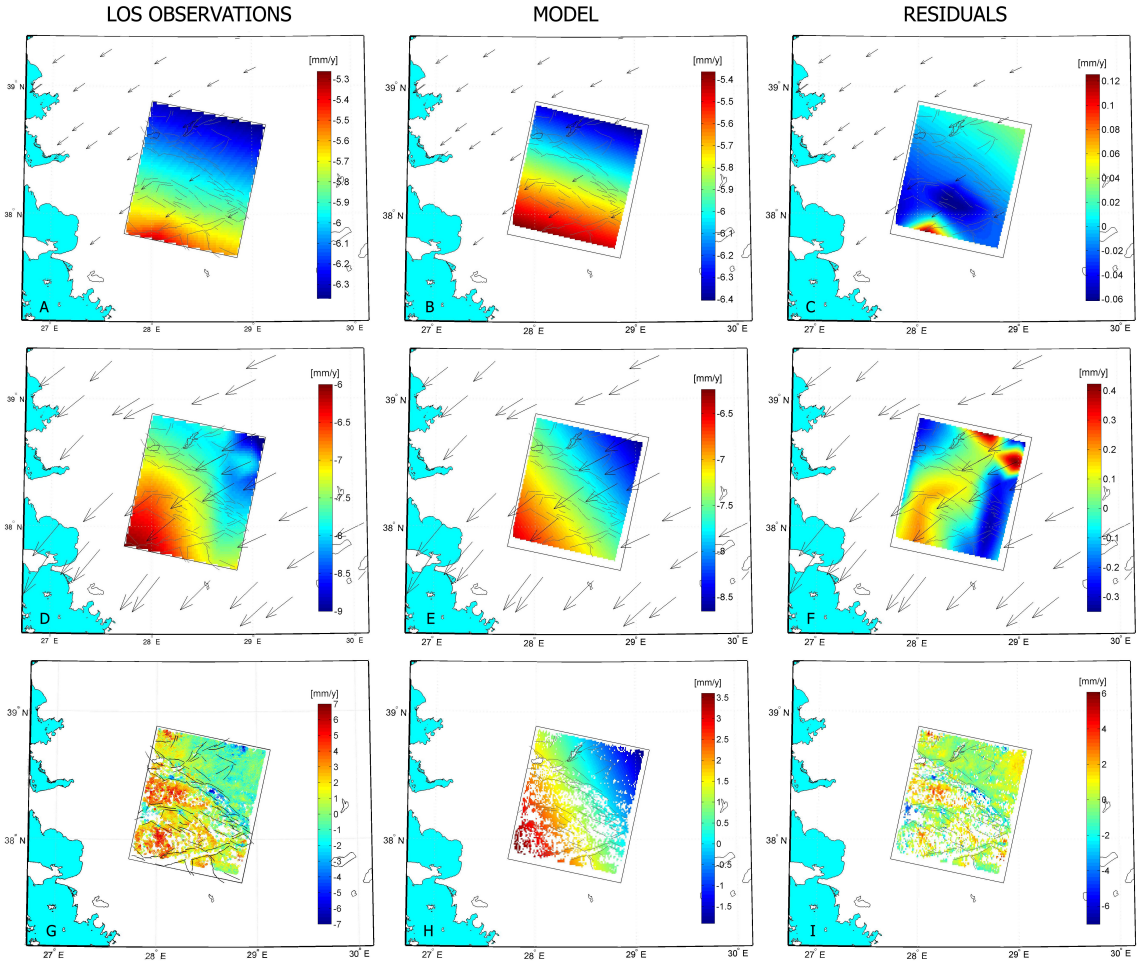

Figure 4. (a,b,c) GPS-1 study: The arrows show the velocity field of GPS measurements with respect to the stable Eurasia, from [12] (1988–2001). (d,e,f) GPS-2 study: The arrows show the velocity field of GPS measurements with respect to the stable Eurasia, from [1] (1997–2006). The color images show the line of sight (LOS) velocity field produced from the GPS measurements for the Descending orbit. (g,h,i) PSI study: The color images show the line of sight (LOS) velocity field estimated using PSI (1992–2000). The black frame depicts the ERS coverage over the grabens. The solid lines represents the normal faults bounding horst-graben structures. The colorbar scales present different magnitudes for each color images.

PS points, then, with oversampled dataset 165374 PS points, and finally eliminating highly decorrelated interferograms from the oversampled dataset 461614 PS points, respectively. Specifically, for the rural areas we have improved our point density.

In both radar line-of-sight displacement of GPS-1 and GPS-2, there is a clear trend in N-S, and NW-SE directions, respectively, By using a simple linear model, we estimate this trend and compute residuals, Figure 4(b) and 4(c), and Figure 4(e) and 4(f), respectively. The total residual values for GPS-1 is $\sim$0.18 mm/yr and for GPS-2 $\sim$0.76 mm/yr. Low residual values indicate that the linear model is a good estimation of the interseismic signal. Using this assumption, similarly, we estimated a linear trend through our PSI estimation. This shows that there is distributed block motion as suggested by [1], however residuals of PSI give more detail on the vertical motion inside the grabens. For example, Ödemiş (Figure 2) and Salihli undergo local subsidence (Figure 5). It is reported that ,especially, for Ödemiş surface cracks occurring due to changes in the water table [4]. Tilting of Ödemiş is clearly visible in Figure 2(b). These areas need further investigation whether the water table change is also controlled by the different permeability of the fault planes. At the eastern side of Gediz graben, there is a basin subsidence that correlates with the location of graben-bounding active faults and seismic observations, see Figures 1(b) and 5. This subsidence is predominantly vertical displacement along the active faults which could be due to interseismic signal, surface creep, and/or due to water pumping.

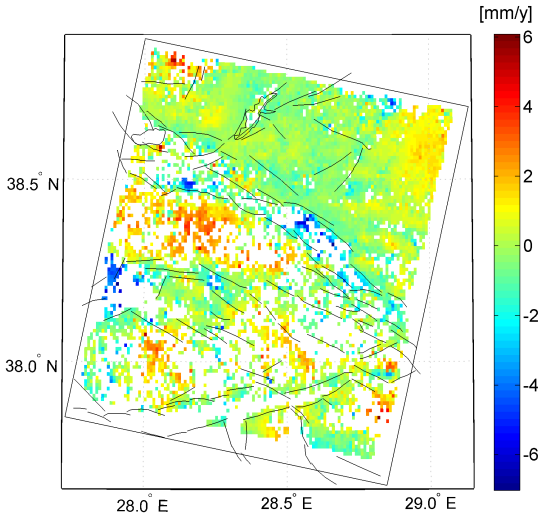

Figure 5. PSI un-modeled signal: The color image shows the line of sight (LOS) velocity field estimated using PSI after removal of the estimated tectonic trend. The black frame depicts the ERS coverage over the grabens. The black lines represents the normal faults.

4. CONCLUSIONS

In this study we have presented our approach to increase coherent target density in the rural areas in order to monitor interseismic tectonic signal. First by considering influence of the phase center alignment and subsequently by identifying and eliminating noisy interferograms.

We applied this approach on the ERS 1/2 acquisitions over 10 000 kilometer square wide area covering major horst-graben structures in West Anatolia. In this area, our GPS modeling results show that the interseismic tectonic signal can be represented as a linear trend. Since GPS studies lack vertical displacement sensitivity and satellite line-of-sight has less sensitivity to North component of the displacement. The modeled interseismic signals, which are estimated from GPS-2 (Aktug et al, 2009) study and our PSI study, show a similar trend direction compared to the model estimated from GPS-1 study. This is perhaps due to the fact that GPS-1 study has a rather sparse network.

On the other hand, PSI observations provide a higher spatial resolution than GPS measurements. This allows us to identify deformation along the grabens bounded by active faults and even subsidence over towns. Conversely, this high spatial resolution allows short wavelength signals to delude our estimation of interseismic signal.

When the long wavelength signal component is estimated and removed from the PSI observations. The remaining signal, predominantly, represents the vertical component of the displacement. This signal could be tectonic when it correlates with the location of the active faults and known seismic activities and/or geophysical parameters. It could also indicate localized displacements due to non-tectonic events such as subsidence due to changes in the water table level.

We expect tectonic and non-tectonic displacements in this study area. Without in-situ information, SAR observations could be an important tool to obtain estimates of interseismic displacements in higher spatial resolution.

Further studies will be conducted to improve our analysis and to estimate geophysical parameters. In a further study we will extend our analysis to the neighboring frames to obtain the tectonic signal on a regional scale.

ACKNOWLEDGEMENTS

The authors would like to thank Joaquim J. M. de Sousa and Miguel Caro Cuenca for valuable discussions during development and implementation of algorithms. We are grateful to The European Space Agency (ESA) for providing ERS data under C1P-4347. Interferometric data were processed using the public domain SAR processor DORIS, DePSI, StaMPS and satellite orbits used are from Delft University of Technology.

REFERENCES

[1] B. Aktug, J. M. Nocquet, A. Cingöz, B. Parsons, Y. Erkan, P. England, O. Lenk, M. A. Gürdal, A. Kilicoglu, H. Akdeniz, and A. Tekgül. Deformation of western Turkey from a combination of permanent and campaign GPS data: Limits to block-like behavior. *Journal of Geophysical Research (Solid Earth)*, 114(B13):10404–+, October 2009.

[2] Mahmut Arikan and Ramon F Hanssen. Structural deformation of the High-Speed Line (HSL) infrastructure in the Netherlands: observations using satellite radar interferometry. In 13^{th} *FIG International Symposium on Deformation Measurements and Analysis, Lisbon, Portugal, 12–15 May, 2008*, Lisbon, Portugal, 2008.

[3] Francesco De Zan and Fabio Rocca. Coherent processing of long series of SAR images. In *International Geoscience and Remote Sensing Symposium, Seoul, Korea, 25–29 July 2005*, 2005.

[4] Ramazan Demirtaş, Müjdat Yaman, and Bengi Eravcı. Surface cracks in western anatolia are earthquake rupture and precursory of a near-future earthquake or surface failure? Case study: Ödemiş-Kınık-Eber-Burdur. In 56^{th} *Geological Congress of Turkey , Ankara, Turkey, 14–20 Apr, 2003*.

[5] J. F. Dewey and A. M. C. Sengor. Aegean and surrounding regions; complex multiplate and continuum tectonics in a convergent zone. *Geological Society of America Bulletin*, 90(1):84–92, January 1979.

[6] Alessandro Ferretti, Claudio Prati, and Fabio Rocca. Permanent scatterers in SAR interferometry. *IEEE Transactions on Geoscience and Remote Sensing*, 39(1):8–20, January 2001.

[7] Andrew Hooper. *Persistent Scatterer Radar Interferometry for Crustal Deformation Studies and Modeling of Volcanic Deformation*. PhD thesis, Stanford University, 2006.

[8] Andy Hooper, Howard Zebker, Paul Segall, and Bert Kampes. A new method for measuring deformation on volcanoes and other non-urban areas using InSAR persistent scatterers. *Geophysical Research Letters*, 31:L23611, doi:10.1029/2004GL021737, December 2004.

[9] B M Kampes. *Displacement Parameter Estimation using Permanent Scatterer Interferometry*. PhD thesis, Delft University of Technology, Delft, the Netherlands, September 2005.

[10] V B H Ketelaar. *Monitoring surface deformation induced by hydrocarbon production using satellite radar interferometry*. PhD thesis, Delft University of Technology, Delft, the Netherlands, September 2008.

[11] S. McClusky, S. Balassanian, A. Barka, C. Demir, S. Ergintav, I. Georgiev, O. Gurkan, M. Hamburger, K. Hurst, H. Kahle, K. Kastens, G. Kekelidze, R. King, V. Kotzev, O. Lenk, S. Mahmoud, A. Mishin, M. Nadariya, A. Ouzounis, D. Paradissis, Y. Peter, M. Prilepin, R. Reilinger, I. Sanli, H. Seeger, A. Tealeb, M. N. Toksöz, and G. Veis. Global Positioning System constraints on plate kinematics and dynamics in the eastern Mediterranean and Caucasus. *JGR*, 105:5695–5720, March 2000.

[12] M. Nyst and W. Thatcher. New constraints on the active tectonic deformation of the Aegean. *Journal of Geophysical Research (Solid Earth)*, 109(B18):11406–+, November 2004.